journal

J. Am. Ceram. Soc., **82** [6] 1529–36 (1999)

Measuring the Influence of Grain-Boundary Misorientation on Thermal Groove Geometry in Ceramic Polycrystals

David M. Saylor* and Gregory S. Rohrer*,†

Department of Materials Science and Engineering, Carnegie Mellon University,
Pittsburgh, Pennsylvania 15213-3890

We have used electron backscattered diffraction patterns to determine the misorientation of 201 adjacent pairs of grains in a magnesia polycrystal. The width and depth of the thermal grooves formed by these same grain boundaries were also measured by atomic force microscopy (AFM). By simulating the errors associated with the AFM observations and comparing our observations to existing data for magnesia and alumina, we show that, under appropriate experimental conditions, surface dihedral angles, relative grain-boundary energies, and surface diffusivities determined from AFM measurements are consistent with data acquired by more laborious techniques. Correlation of the grain-boundary misorientation and thermal groove geometry leads to the observation that grain boundaries with small misorientations, regardless of the rotation axis, have shallow thermal grooves and relatively low grain-boundary energies. Furthermore, numerous boundaries with relatively large misorientations but shallow thermal grooves correspond to special boundaries near coincident-site-lattice (CSL) misorientations. Finally, the data set indicates that factors other than the boundary misorientation, such as anisotropy of the surface energy and the grain-boundary tangent plane, play a role in determining the groove geometry.

I. Introduction

The most common way to experimentally probe relative grain-boundary energies is to measure the geometry of the thermal grooves that form where the boundaries intersect a free surface. The relationship between the interfacial geometry and the interfacial energies was first quantified by Herring,[1] who reasoned that, if the line where a grain boundary meets two free surfaces is stationary and in local equilibrium, the forces exerted on this junction by the three interfaces must sum to zero. This force balance is expressed in the following equation.

$$\gamma_i \mathbf{t}_i + \mathbf{n}_i \frac{\partial \gamma_i}{\partial \theta} = 0 \tag{1}$$

Here, γ_i is the excess free energy per unit area of the ith interface; $\mathbf{t}_i$ the unit vector that lies in the ith interface and is normal to the line of intersection of the three interfaces (l); and $\mathbf{n}_i$ the unit vector normal to the line of intersection, such that $\mathbf{n}_i = \mathbf{t}_i \times l$. The configuration of these vectors is illustrated in Fig. 1(a). In principle, it is possible to completely determine the interfacial energies by observing the geometry of a sufficient number of interfaces among crystals of known orientation. For example, if the interfacial energies are represented as Fourier series or expansions of lattice harmonics, then these functions can be determined by fitting observed geometric and orientational parameters to a set of unknown coefficients. Until recently, this approach was experimentally impractical in all but a limited number of cases for which samples with a model microstructure could be fabricated.[2,3] As a result, the existing measurements on ceramics are rather limited in scope,[4–14] and experimental data have been analyzed under the assumptions that the so-called torque terms, $\partial\gamma_i/\partial\theta$ in Eq. (1), are negligible; that the surface energy is isotropic; and that the grain-boundary energy is a function of its misorientation but not of its tangent plane. Under these conditions, Eq. (1) reduces to:

$$\frac{\gamma_{gb}}{\gamma_s} = 2 \cos \frac{\psi_s}{2} \tag{2}$$

In Eq. (2), the ratio of the grain-boundary excess free energy to the surface excess free energy (γ_{gb}/γ_s) is a function of the experimentally measured surface dihedral angle of the groove, ψ_s.

In past studies of relative grain-boundary energy, data have been collected both from boundaries in model bicrystalline specimens[4–10] and from boundaries in sintered polycrystals.[11–14] The advantage of studying bicrystals is that the misorientation among the two crystallites, the grain-boundary plane, and the indexes of the free surfaces are all defined by the conditions of the experiments or by theoretical models. Therefore, the dependence of the grain-boundary-to-surface energy ratio on the misorientation angle can be determined. However, because bicrystal fabrication is labor-intensive, such data usually are limited to a few low-index rotation axes. Although the studies of polycrystals potentially sample a much wider range of misorientation space, the existing data are limited to median values of the grain-boundary-to-surface energy ratio determined from distributions of randomly selected boundaries with unknown misorientations.

The objective of the present paper is to describe a facile method of measuring the geometry of thermal grooves in sintered polycrystals and the misorientation of the adjoining crystallites. Thermal groove geometries are determined by atomic force microscopy (AFM), and crystallite orientations are determined using orientation imaging microscopy (OIM).[15] Using such data, it is possible to specify the misorientation dependence of the grain-boundary-to-surface energy ratio. After describing the procedures used for our measurements, we compare the distribution of angles that we observed in alumina and magnesia, using AFM, with those measured by the metal reference line (MRL) technique.[13] We then describe the misorientation dependence of the grain-boundary-to-surface energy ratio in magnesia. Although the energy ratios have been calculated using Eq. (2), the results suggest that it is possible to analyze more extensive data using Eq. (1), so that both the grain-boundary and surface energies can be determined without neglecting anisotropy and the contributions from the torque terms.

T. E. Mitchell—contributing editor

Manuscript No. 190283. Received March 31, 1998; approved September 21, 1998.
Supported primarily by the MRSEC Program of the National Science Foundation under Award No. DMR-9632556.

*Member, American Ceramic Society.

†Author to whom correspondence should be addressed.

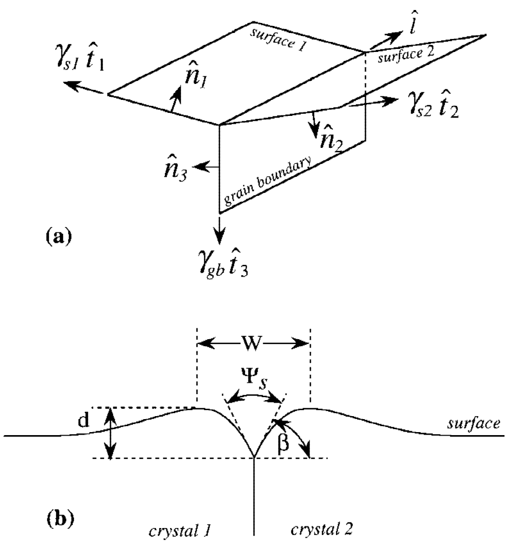

Fig. 1. Schematic geometry of the thermal groove. (a) Local view of a triple line, where two free surfaces and a grain boundary meet; quantities in Eq. (1) are depicted. (b) Projection, parallel to *l*, illustrating schematic macroscopic structure of surface thermal groove. Aspect ratio of the groove is exaggerated for clarity. Labeled dimensions are described in the text.

II. Experimental Procedure

(1) Sample Preparation

The alumina samples used in the present study were made from 99.99% pure alumina powder (AKP-50, Sumitomo Chemical America, Inc., New York). The powder was compacted mechanically in a uniaxial press at 28 MPa and then isostatically pressed at 280 MPa to form disk-shaped pellets 25 mm in diameter and averaging 2.4 mm thick. The pressed pellets then were packed in an alumina crucible with the parent powder and fired for 5 h in air at 1600°C. This process provided samples with a relatively small grain size (3.2 μm) that were used to study grooving kinetics. After the samples had been sintered, the surfaces were ground and polished mechanically, using diamond suspensions, down to a diamond particle size of 0.25 μm. The grain boundaries of these samples then were thermally grooved in air at 1400°C, and selected boundaries were examined repeatedly by AFM after 1, 2, 3, 4, 6, 8, 10, and 20 h of annealing.

A second set of samples, from which the dihedral angle distribution was determined, were processed in a similar fashion. In this case, the same powder was compacted mechanically in a uniaxial press at 76 MPa to form disk-shaped pellets 10.5 mm in diameter and averaging 2.3 mm thick. The pellets then were packed in an alumina crucible with the parent powder and fired for 25 h in air at 1700°C. The average grain size in these samples, as determined by the linear intercept method, was 8.0 μm. After the samples had been ground and polished, thermal grooving was conducted in a conventional box furnace. To minimize contamination from the refractories, the samples were contained in a single-crystal sapphire crucible and surrounded by the parent powder. A heat treatment of 1 h yielded grooves with an average width of 2.3 μm.

Magnesia powder was formed by decomposing 99.7% pure magnesium carbonate (Fisher Scientific Co., Pittsburgh, PA) at 997°C in air. The calcined powder was compacted uniaxially at 76 MPa and then isostatically at 276 MPa, to form disk-shaped pellets 20.0 mm in diameter and averaging 2.8 mm thick. The disks then were packed in a magnesia crucible with the parent powder and sintered for 48 h in air at 1600°C. After the samples had been sintered, the surfaces were ground and polished mechanically, using diamond suspensions, down to a diamond particle size of 0.25 μm. Thermal grooves were formed by annealing the polished samples for 5 h in air at 1400°C. These anneals were conducted in air in a conventional box furnace. The samples were enclosed in a magnesia crucible and surrounded by the parent powder. The average grain size of these samples was 40 μm, and the average width of the thermal grooves was 2.4 μm.

(2) AFM Imaging

The microscope used in this study was capable of making topographic, contact AFM images at any point on a sample surface within a 6.25 cm^2 area. This instrument (a StandAlone AFM, Model SAA-125, Digital Instruments, Tonawanda, NY), positioned above the sample mounted on an *X-Y* translation stage (Model TSE-150, Burleigh Instruments, Fishers, NY), was capable of reproducibly positioning the sample with 50 nm resolution. The advantage of this system was that, once a coordinate system and reference frame were established (with respect to an intentionally introduced fiducial mark), it was possible to return to identical positions on the sample surface after repeated thermal treatments or to position the sample based on lower-resolution data from the AFM or other microscopes. Silicon nitride cantilevers (Model LNP, Digital Instruments) were used as probes.

The factors that potentially contribute to errors during an attempt to make quantitative geometric measurements with an AFM include the scanner calibration, the information density of the image, the definition of the surface normal, the background subtraction, and the convolution of the tip shape with the sample surface. Each of these experimental factors, and the procedures used to minimize its impact, is described briefly below.

The lateral and vertical calibrations for our AFM were established using a lithographically produced standard grating supplied by the manufacturer. The calibration was checked for consistency with the scanners on other microscopes in our laboratory, which have been calibrated using surface crystallographic features.[16] The second consideration was the information density of the images from which the measurements were made. The topographic data were collected pixel-by-pixel, and the lateral resolution limit was determined by the pixel spacing. Groove measurements were made using images composed of 512 lines, with 512 pixels per line, and linear dimensions of 4–10 μm. Therefore, the lateral resolution limit was between 8 and 28 nm, and the shape of each groove was defined by a minimum of 80 pixels. Typically, groove traces consisted of several hundred pixels. In the vertical dimension, height differences of <1 nm typically were resolved.

The objective of the present study was to measure topographic deviations from the average surface plane, and so it was important that the sample have flat, parallel surfaces and that the surface be parallel to the AFM scanning plane. Because the AFM scanning plane was somewhat arbitrary, in that it could be altered with the instrumental tilts, we made sure that the sample had two flat, parallel surfaces before the measurement. These surfaces were achieved by polishing the sample in a piston-style mount and measuring the deviations from planarity using an inductive axial movement gauge head (Model GT22, TESA Measurement Systems, Novi, MI) with a resolution of 0.1 μm. Based on these macroscopic measurements, the samples used for the thermal groove measurements were flat to ±2.5 μm over lateral distances of 1 cm. After the sample was mounted onto the AFM stage, the flat surface then served as a reference plane, and the instrumental tilts were adjusted so that the angle between the sample surface plane and the image plane was less than 1° over a 100 μm scan area.

It is especially important to base geometric measurements on uncorrected topographic data. Many AFM operating systems automatically subtract background planes, an operation that distorts the actual topography. The only background subtraction used for our measurements is a constant offset applied equally to each pixel. This operation is used to center the contrast range and does not distort the topography. The convolution of the AFM probe shape with the sample surface topography is a well-known problem in AFM imaging. This problem is greatest during attempts to measure concave shapes, such as grain-boundary grooves.

The central issue is illustrated in Fig. 2. As the AFM probe descends into the groove, its vertical position is actually determined by a point on the side of the tip, not by the point at the end of the tip. For relatively steep and/or narrow grooves, this determination leads to a systematic underestimation of the depth and slope. The magnitude of this systematic error depends on the aspect ratios (width to depth) of the groove and the tip. It is possible to determine the systematic errors associated with measuring specific shapes with specific probes[17–19] by using established simulation methods. Thus, we have the choice of either correcting the observed data or finding domains for the experimental parameters in which the errors are small enough to be tolerated.

To explore the errors involved in measuring grooves by AFM, we used the envelope reconstruction simulation method.[17] We began by developing model surface groove topographies with a variety of dihedral angles and widths, using the solution to the quasi-static groove profile developed by Mullins.[20] Although the ideal Mullins groove shape is convenient to use, it does not accurately describe the shapes of grooves with small surface dihedral angles ($\psi_s < 140°$). Robertson's[21] numerical determination of the quasi-static groove profile shows that, for a given dihedral angle and groove width, the profile predicted by the Mullins[20] equation is too deep. In other words, the Mullins shape is actually more challenging to measure than the expected groove shape. Thus, by simulating profiles measured from the Mullins[20] groove profile, we were certain of obtaining an upper limit for the systematic error.

Our two-dimensional model probe tip is a triangle with an inner angle of 35° capped by a circle with a radius of 60 nm (probes with smaller inner angles are commercially available but not as robust). This shape conforms to the maximum size specified by the manufacturer and is consistent with high-resolution SEM images of probe tips after use.

Again, we chose the most pessimistic dimensions because we were interested in determining the maximum error. Based on simulated images of predefined grooves that spanned the range of expected geometries, we calculated the error in the measured groove width, *W*; groove depth, *d*; and groove angle, β. (These parameters are defined in Fig. 1(b).) The results, summarized in Fig. 3, show that the error in β, determined from measurements of *d* and *W*, decreased as the groove width increased.

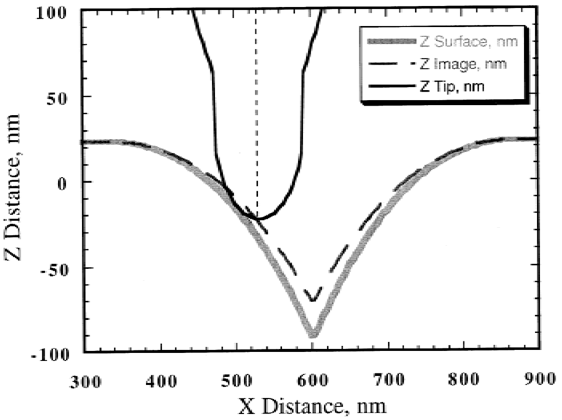

Fig. 2. Illustration of why AFM topographs systematically underestimate the depths of narrow, deep grooves. Because the point at which the tip contacts the groove surface is not on the tip axis, the slope of the concave shape and its depth are systematically underestimated. Vertical axis is amplified with respect to the horizontal axis; this aspect ratio distorts the actual shape of the tip, which has an inner angle of 35°.

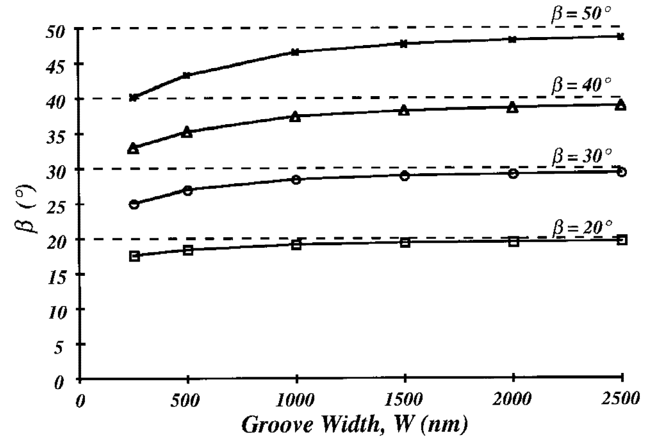

Fig. 3. Comparison of the values of the angle β, determined from measurements of *W* and *d*, with actual values for model thermal grooves of different width (*W*) and angle, β. As the grooves become wider, the measured and actual values converge.

Based on the results of the simulations, we drew the following conclusions. First, the convolution of the tip shape and the surface topography did not create an error in our measurement of the groove width, *W*. Second, the inner angle of the tip limited the range of dihedral angles that could be measured reliably to $\beta \leq 55°$ ($\psi_s \geq 70°$). However, based on previously reported measurements of dihedral angles, we expected the population of inaccessible boundaries to be very small or nonexistent.[13] Finally, as the boundary width increased, both the depth (*d*) and the angle (β) were measured with acceptable accuracy. Based on these results, we confined our observations to grooves with an average width >2 μm.

Determining the dihedral angle from measurements of *d* and *W*, rather than from direct measurements of β, eliminates the errors associated with measuring the slope. To compute β, we must determine the slope from at least 10 pixels near the groove root. Because the slope continuously decreases with distance from the groove root, the averaging necessary for calculating a slope leads to a systematic underestimation of β. This result is essentially the same problem analyzed by Handwerker *et al.*[22] for groove measurements using other techniques. We can eliminate this particular source of error by computing β based on the known relationship between *W* and *d* determined by Robertson.[21] Although a systematic error in the measurement of *d* remains, the simulation results show that it is relatively small.

Specifically, the present simulation results showed that, in the worst case, we underestimated the depth of a 2 μm wide groove by less than 5%. The most challenging geometry encountered in our study was a boundary with $\psi_s = 82°$ and $W = 2.2$ μm. Our simulations showed that, for such a boundary, the maximum error in ψ_s was 4°, which corresponds to an error in γ_{gb}/γ_s of 0.05. At the median of the observed distribution ($\psi_s = 105°$ and $W = 2.4$ μm), the errors in ψ_s and γ_{gb}/γ_s were 2° and 0.03, respectively. Because we made assumptions that tended to maximize the estimated error, the real errors derived from the convolution of the tip and groove shape actually must have been smaller.

In summary, consideration of the potential systematic errors led us to the following procedure for determining surface dihedral angles. First, the specimens were polished so that they had two flat, parallel surfaces. Second, thermal treatments were used to groove the surfaces, so that the average width was at least 2 μm. Before collecting data, the AFM was adjusted so that the image plane was parallel to the surface plane. Based on low-resolution maps of the surface, the *X-Y* translation stage was used to seek triple junctions, such that AFM topographs, 4–10 μm on each side, could be recorded with an information density of 512 pixels per row and 512 rows. In each image, the triple junction was centered so that there were three grain boundaries. We then measured the geometry of each boundary by selecting linear traces over each of the three boundaries and searching the traces for maximum and minimum points at each groove. This procedure is illustrated graphically in Fig. 4.

Using three traces over each boundary provided three measurements of W and d for each groove, which were averaged to yield final values from which the surface dihedral angle was determined. In several cases, we made 10 measurements of W and d at different positions along boundaries with some curvature, where there were potential differences in the indexes of the free surfaces bounding the groove and in the grain-boundary tangent plane. Based on such measurements, we estimated that the standard deviation resulting from measuring different positions in the same groove was 4° in ψ_s. When this process was repeated on straight boundaries, where all three of the interfaces bounding the groove remained constant, the standard deviation associated with the random errors in our measurement procedure was 1° in ψ_s for each boundary.

(3) Determining Grain Orientations

The grooved samples examined by AFM also were imaged (uncoated) in a scanning electron microscope (Model XL40FEG, Philips Electronic Instruments, Mahwah, NJ). Using fiducial marks on the sample, we located the grains examined by AFM and obtained electron backscattered diffraction patterns (EBSP) for each grain (examples are illustrated in Fig. 4). The patterns were obtained either by pointing the beam directly at individual grains or by scanning the beam systematically over a selected area and recording a diffraction pattern at each point. All of the patterns were indexed using orientation imaging microscopy software (version 2.5, TexSEM Laboratories, Inc., Draper, UT), which returned a set of Euler angles for each grain. The Euler angles from adjacent grain pairs then were used to define the misorientation by deriving the pair's common axis and the rotation angle about the axis that brought the crystallites into coincidence.

Following convention, the axis/angle representations of misorientation were parameterized as Rodrigues vectors, where the vector lies in the direction of the misorientation axis and has a magnitude that scales with the misorientation angle.[23] By imposing the conditions that the rotation axis lay in the standard cubic stereographic triangle and the rotation angle was as small as possible, we obtained the symmetrically equivalent Rodrigues vectors that lay in an irreducible wedge of cubic misorientation space (also referred to as the MacKenzie cell).[24,25]

III. Results

(1) Misorientation Averaged Results

Figure 5 shows the distribution of dihedral angles that we observed for alumina (Fig. 5(a)) and magnesia (Fig. 5(b)), as determined from AFM measurements of W and d. In the past, various techniques have been used to measure thermal grooves on similar samples. These data were reviewed by Handwerker *et al.*,[13,22] who showed that systematic errors in the measurement decreased as the resolution increased.

Thus, the most reliable preexisting measurements are based on MRL observations. Handwerker *et al.*[13,22] corrected the MRL observations to account for the resolution limit of the technique, and we have plotted the corrected data for comparison in Fig. 5. The median values of the distributions measured by AFM and the MRL techniques are the same, 106° for alumina and 105° for magnesia. However, there are some differences in the shapes of the distributions.

We also examined the kinetics of groove formation in alumina to see if our AFM observations were consistent with earlier studies. The AFM images in Fig. 6 show the same region of the surface at different times (1, 6, and 10 h) during an anneal at 1400°C. As the annealing time increased, the boundaries became deeper and wider, and the facets on the grain surfaces coarsened. At intervals of 1, 2, 3, 4, 6, 8, 10, and 20 h, during an anneal at 1400°C, the widths of three different boundaries were monitored. While depth measurements of such narrow boundaries would be unreliable, the width measurement was unaffected by the tip/groove convolution.

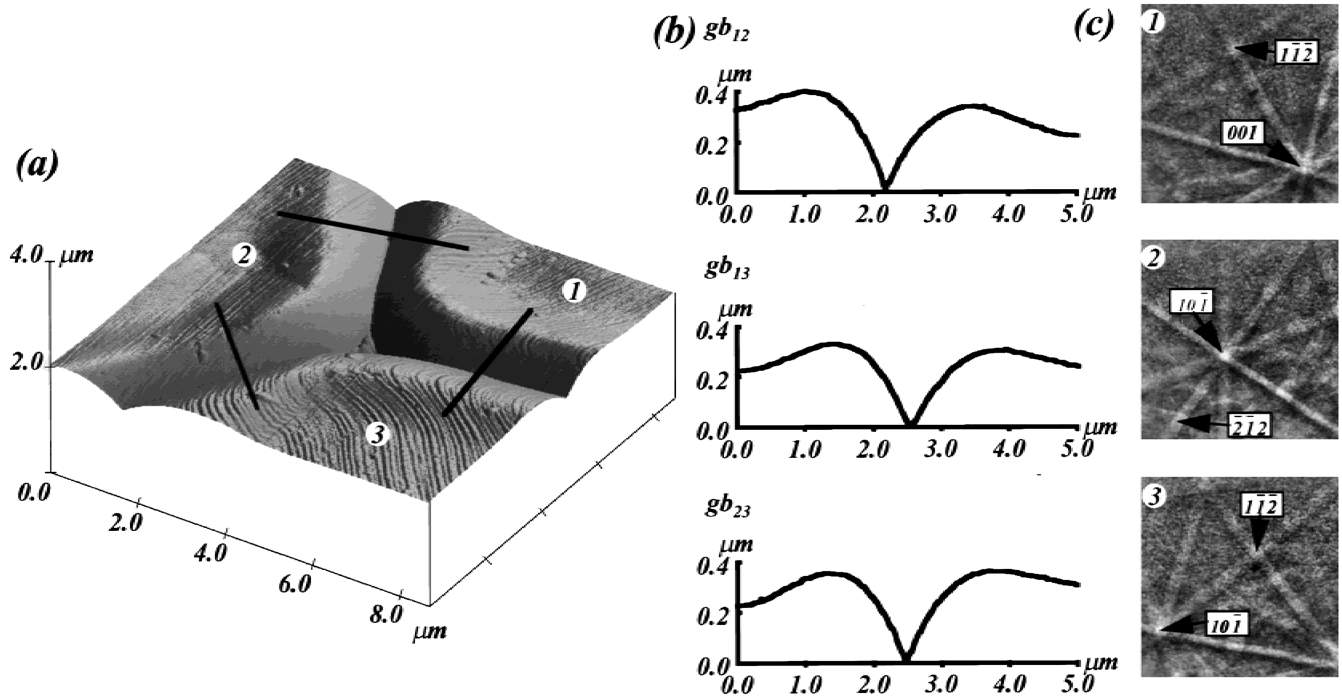

Fig. 4. (a) Typical contact AFM image of the point where a triple junction intersects the surface of a magnesia polycrystal. Black lines show the locations at which the three topographic traces in (b) were obtained. Values of W and d are obtained from each trace; final values of W and d are determined by averaging three measurements from profiles at different locations on each groove. Standard deviation of the data acquired in this manner is 4°. (c) EBSP for each grain labeled in (a); these data are used to determine the misorientation.

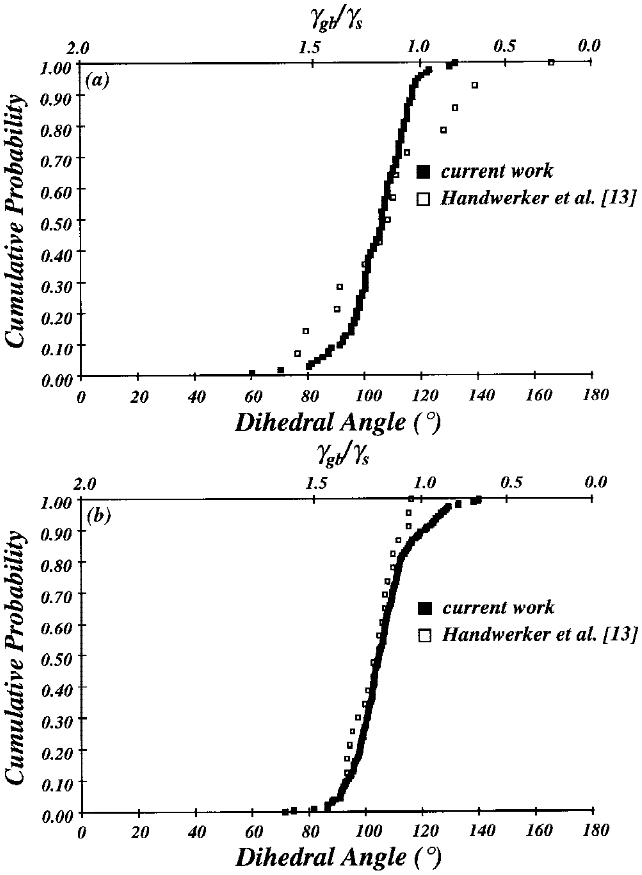

Fig. 5. (a) Distribution of thermal grooves in alumina etched for 1 h at 1600°C, in air. (b) Distribution of thermal grooves in magnesia etched for 5 h at 1400°C, in air. For comparison, equivalent data from Ref. 13 are plotted on each graph.

Mullins[20] showed that the quasi-static groove profile depends on the atomic removal mechanism and that the slope (m) of an ln (W) versus ln (time) plot can be used to differentiate among surface-diffusion ($m = 0.25$), volume-diffusion ($m = 0.33$), and evaporation/condensation ($m = 0.50$) mechanisms. The time dependence of the width of three separate grooves is illustrated in Fig. 7. The slopes of the three curves ($m = 0.21$, 0.24, and 0.24) are closer to the slope predicted when a surface-diffusion mechanism ($m = 0.25$) is assumed, rather than the alternatives.

Assuming that the grooves are formed by surface diffusion, the groove width data can be used to compute a surface-diffusion coefficient. Based on Mullins'[20] analysis, the surface diffusion coefficient (D_s) is given by the following equation.

$$D_s = \frac{W^4 kT}{4.6^4 \gamma_{sv} \Omega^2 N t} \tag{3}$$

Surface-diffusion data for alumina have been reviewed previously by Tsoga and Nikolopoulos.[14] The constants from Eq. (3) were taken from this earlier work, to facilitate a comparison with the current data. Specifically, the molecular volume (Ω) is 2.11×10^{-23} cm^3/molecule, the surface energy (γ_{sv}) is 1.25 J/m^2, and the number of diffusing species (N) is $\Omega^{-2/3}$; k and T are Boltzmann's constant and the absolute temperature (1673 K), respectively.

Tsoga and Nikolopoulos[14] used optical measurements to determine the groove width as a function of time and, based on their findings, D_s at 1400°C in air should be 4.9×10^{-9} cm^2/s. This number was computed based on average widths and ignores the anisotropy of the surface energy and diffusivity. Results from other groups were cited in the same paper, and when extrapolated to 1400°C, they vary from 5×10^{-10} to 1×10^{-7} cm^2/s. The widths from the three boundaries we measured led to surface-diffusion coefficients of 9.4×10^{-10}, 1.4×10^{-9}, and 5.3×10^{-11} cm^2/s. The average of these three numbers falls in the lower end of the range observed in past studies.[14]

The scatter in our measurements from different boundaries probably indicates the anisotropy of the surface diffusivity and/or surface energy. The lowest of our three values, which derives from a shallow, narrow boundary, falls outside the range of previous observations. However, because of its size, such boundaries would be overlooked in an optical study. After 20 h of annealing, the width of this particular boundary is <500 nm, one-half the size of the smallest boundary reported in the earlier work.

(2) The Effect of Grain-Boundary Misorientation

The surface dihedral angle data can be used to represent the γ_{gb}/γ_s ratio as a function of misorientation. As described earlier, we represent the misorientation between two grains as a Rodrigues vector, with components $R1$, $R2$, and $R3$, in the irreducible wedge of cubic misorientation space. The distribution of observed grain boundaries in the irreducible wedge is shown in Fig. 8. Each point in the plot represents an observed grain boundary, and the points are shaded in proportion to the size of the γ_{gb}/γ_s ratio. The darkest points correspond to the lowest values, whereas the brightest correspond to the highest values. Based on the cluster of data near the origin, a large fraction of boundaries have small misorientations (the magnitude of the Rodrigues vector is small). In other words, there is a high population of low-angle grain boundaries in this sample. Furthermore, because most of these points have a relatively dark shading, these boundaries have the lowest relative values of the γ_{gb}/γ_s ratio. Thus, the low-angle boundaries must have a relatively low energy.

IV. Discussion

It is important to verify that the AFM measurements described here lead to results consistent with those of previous studies using accepted techniques. Handwerker *et al.*[22] published a detailed discussion of the errors associated with determining surface dihedral angles by optical microscopy, optical interferometry, and SEM. Their analysis showed that such measurements systematically overestimate the true surface dihedral angle and that the error diminishes as the resolution limit increases. Based on this analysis, Handwerker *et al.*[22] estimated that the median dihedral angles observed by MRL in alumina and magnesia were 9° and 7° larger, respectively, than the true median value. These corrected data sets are included in Fig. 5.

The error analysis method used by Handwerker *et al.*[22] does not apply directly to AFM images, because the vertical resolution in a topograph is many times greater than the horizontal resolution. For this reason, we used envelope reconstruction simulation methods to determine the maximum errors in our observations. For wide grooves, our maximum systematic errors were lower than the random errors associated with the process.

Wide grooves are more accurately measured than narrow ones, simply because as a groove becomes wider and deeper, the absolute error in d remains approximately constant, and this error is a diminishing fraction of the total. The resolution advantage of AFM comes not from the measurement of W (the lateral resolution is similar to that from SEM), but from the measurement of d, where the AFM is capable of resolving differences in depth <1 nm. In any case, the similarity of the MRL and AFM results illustrates an acceptable degree of consistency.

Surface-diffusivity data derived from AFM observations also are consistent with accepted data. The most significant advantage of the AFM technique is that it is much less labor-intensive and, therefore, allows more boundaries to be sampled. Several hundred boundaries can be measured easily in a time scale of days.

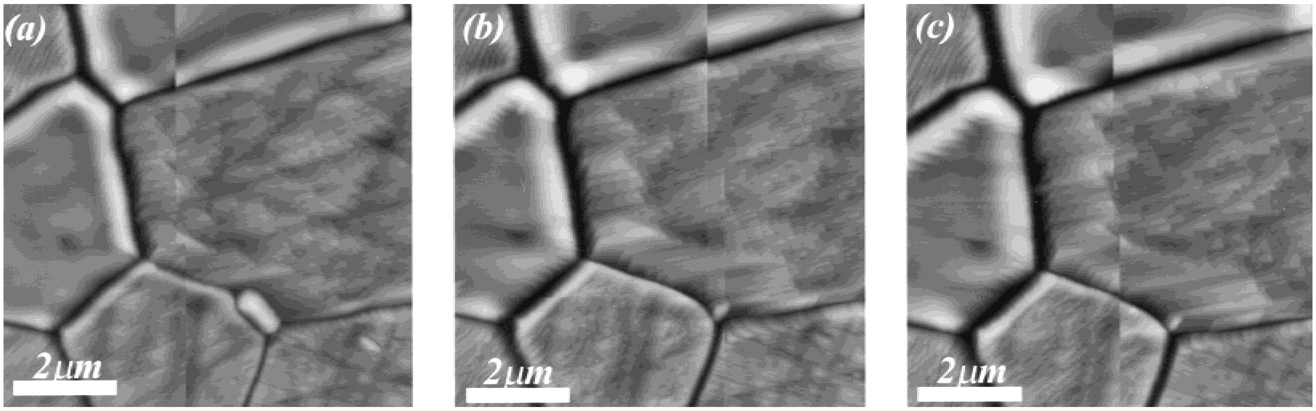

Fig. 6. AFM image montages of the same area of an alumina surface after annealing for (a) 1, (b) 6, and (c) 10 h at 1400°C. In all images, vertical contrast from black to white is 100 nm. Contrast discontinuities occur at the boundaries between separate images with different average contrast levels.

Although the AFM and MRL results give the same median values for the dihedral angle distribution, there are some noteworthy differences in the details of the distribution. For example, the AFM-measured magnesia distribution is wider on both sides of the median. There are several potential sources for the differences. The first source might be the number of points in each distribution. For alumina, there are 14 MRL observations and 101 AFM observations. Similarly, for magnesia, there are 23 and 201 observations for MRL and AFM, respectively.

The second potential reason for the differences might be related to sample purity and texture. For example, the alumina samples examined by Handwerker *et al.*[13] were sintered under vacuum. The alumina samples described here were sintered in air and might, therefore, have had a greater impurity concentration. The relatively large number of low-angle boundaries detected in our magnesia specimen might have resulted from crystallographic texture introduced during processing. The sample described here had a ⟨111⟩ texture, measured by OIM to be 6.5 times random, whereas the texture of the samples examined by MRL was not reported.

The influence of grain-boundary misorientation on the geometry of the thermal grooves on magnesia surfaces was examined under the assumptions that the torque terms were negligible, the surface energy isotropic, and the grain-boundary energy insensitive to its tangent plane. Interestingly, even with such sweeping assumptions, there were clear trends in the data. For example, grain boundaries with small misorientations had the largest surface dihedral angles, indicating that γ_{gb}/γ_s was small. This result was consistent with the idea that small misorientations could be accommodated by relatively minor atomic displacements in the boundary, so that the boundary energy was low.

In addition to the low-angle boundaries, a number of high-angle boundaries (misorientations $\geq 10°$) had unusually low γ_{gb}/γ_s ratios in the present study. For example, eight high-angle boundaries in our distribution had γ_{gb}/γ_s ratios more than one standard deviation below the mean. We compared these boundaries to the known 47 CSL boundaries, with values of $\Sigma \leq 49$,[26] and found that three of them had rotation axes within 3° and misorientation angles (ω) within 2.4° of a coincident-site-lattice (CSL) misorientation. These boundaries included a $\Sigma 7$, a $\Sigma 17b$, and a $\Sigma 45a$. At slightly higher γ_{gb}/γ_s ratios, but still below the mean, an additional five near-CSL boundaries were detected. The observed near-CSL boundaries are listed in Table I.

Although the simplified analysis used in the current paper explains most of the data, some additional features are probably best explained by the anisotropy of the surface energy or the influence of the grain-boundary tangent plane on its energy. For example, two boundaries in the data set have very nearly the same misorientation (the axes of rotation are separated by only 4.2°, and the rotations differ by only 0.4°), yet the values of γ_{gb}/γ_s are 1.4 and 0.9. Assuming that the energies of these two grain boundaries are similar, the difference in the γ_{gb}/γ_s ratio might be caused by the anisotropy of γ_s. The shallow groove is bounded by surfaces near (100) and (221), whereas the deeper groove is bounded by surfaces near (100). Calculations of the surface energy of magnesia predict that the (100) surface has the minimum γ_s, and as the surface normal rotates from (100) to (110), the surface energy increases from 1 to 3 J/m^2.[27] Assuming this increase is true, then the low surface energy of the (100) surface might explain the relatively higher value of the γ_{gb}/γ_s ratio. In addition, the different surface traces of the two grain boundaries indicate that they must also have different tangent planes. Although this effect might contribute to the discrepancy in the observations, its sign or magnitude is difficult to estimate based on existing data.

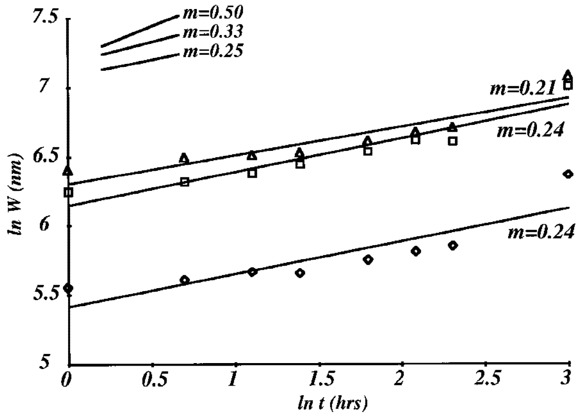

Fig. 7. Time (t) evolution of groove width (W) for three grooves on an alumina polycrystal heated in air at 1400°C. Slopes of the lines indicate that the dominant atomic removal mechanism is surface diffusion.

Because groove geometries are influenced by the anisotropy of the surface energy and/or the grain-boundary tangent plane, it should be possible to measure these factors. To do so necessitates determining partial dihedral angles, a step that requires knowledge of the grain boundary's inclination with respect to the free surface. Preliminary tests in our laboratory have demonstrated that it is possible to measure this inclination through calibrated serial sectioning. Because the techniques described in the present paper allow numerous measurements to be recorded in a relatively short time, we should be able to analyze a more extensive data set, using techniques similar to those

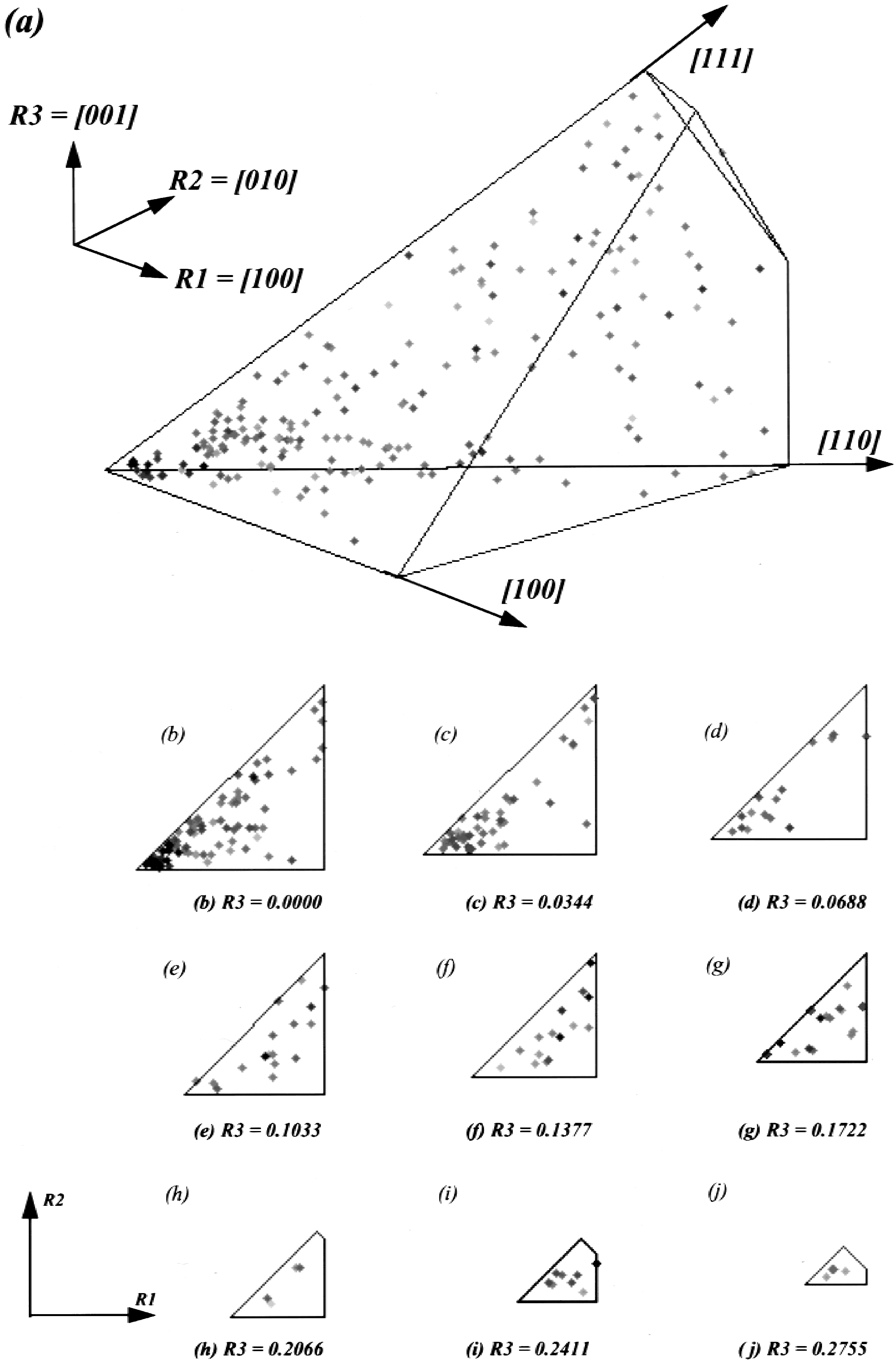

Fig. 8. Distribution of observed boundaries in an irreducible wedge of cubic misorientation space. Shading of each point corresponds to the γ_{gb}/γ_s ratio for that boundary. There are 10 shades of gray, with a resolution of 0.1 in γ_{gb}/γ_s, ranging from 0.7 (darkest) to 1.7 (lightest). (a) Oblique projection of the three-dimensional wedge and (b)–(j) progressive slices of the wedge along the *R*3 or [001] axis. Value of *R*3 listed below each slice indicates bottom coordinate of the slice.

Table I. Relative Grain-Boundary Energies of Near-CSL Boundaries in MgO

Σ	$\langle hkl \rangle$	ω (°)	$\langle hkl \rangle$ Misorientation (°)	ω (°) Misorientation (°)	γ_{gb}/γ_s
5	100	36.86	3.65	0.73	1.1
7	111	38.21	1.14	1.87	1.0
17b	221	61.92	2.87	1.19	0.9
21b	211	44.41	3.13	1.76	1.1
25b	331	51.68	4.76	1.95	1.1
33c	110	58.99	4.17	0.23	1.1
37c	111	50.57	4.55	1.53	1.1
45a	311	28.62	3.00	2.33	1.0

recently proposed by Adams *et al.*,[28] without neglecting the effects of the torque terms, the anisotropy of the surface energy, or the influence of the grain-boundary tangent plane.

V. Conclusions

AFM is a facile method for determining the geometries of grain-boundary grooves. Relative grain-boundary energies calculated from these data are consistent with accepted values. When the relative grain-boundary energy is correlated with the grain-boundary misorientation, boundaries with small or near-CSL misorientations have lower relative energies. However, the data set also reveals that factors other than misorientation determine groove geometry. Assuming that these other factors are the anisotropy of the surface energy and the effect of the grain-boundary tangent plane on the grain-boundary energy, it should be possible to measure both of these quantities by characterizing in detail both the geometry and the misorientation of the boundaries.

Acknowledgments: The authors thank D. Kovar for the fine-grained alumina sample used for the measurement of grooving kinetics and acknowledge fruitful discussions with W. W. Mullins and A. Morawiec.

References

[1] C. Herring, *The Physics of Powder Metallurgy*; pp. 143–79. Edited by W. E. Kingston. McGraw Hill, New York, 1951.

[2] M. McLean and B. Gale, “Surface Energy Anisotropy by an Improved Thermal Grooving Technique,” *Philos. Mag.*, **20** [167] 1033–45 (1969).

[3] B. Gale, R. A. Hunt, and M. McLean, “An Analysis of Surface Energy Anisotropy Data Using Lattice Harmonics,” *Philos. Mag.*, **25** [4] 947–60 (1972).

[4] R. L. Moment and R. B. Gordon, “Energy of Grain Boundaries in Halite,” *J. Am. Ceram. Soc.*, **47** [11] 570–73 (1964).

[5] D. W. Readey and R. E. Jech, “Energies and Grooving Kinetics of [001] Tilt Boundaries in NiO,” *J. Am. Ceram. Soc.*, **51** [4] 201–208 (1968).

[6] J. F. Shackelford and W. D. Scott, “Relative Energies of Tilt Boundaries in Aluminum Oxide,” *J. Am. Ceram. Soc.*, **51** [12] 688–91 (1969).

[7] D. Wolf, “Effect of Fe^{2+} Substitutional Impurities on the Stability of a Σ = 5(100) CSL Twist Boundary on MgO: A Theoretical Study”; pp. 36–43 in Advances in Ceramics, Vol. 6, *Character of Grain Boundaries*. Edited by M. F. Yan and A. H. Heuer. American Ceramic Society, Columbus, OH, 1983.

[8] G. Dhalenne, M. Dechamps, and A. Revcolevschi, “Energy of Tilt Boundaries and Mass Transport Mechanisms in Nickel Oxide”; pp. 139–50 in Advances in Ceramics, Vol. 6, *Character of Grain Boundaries*. Edited by M. F. Yan and A. H. Heuer. American Ceramic Society, Columbus, OH, 1983.

[9] D. M. Duffy and P. W. Tasker, “Properties of Grain Boundaries in Rock Salt Structured Oxides”; pp. 275–89 in Advances in Ceramics, Vol. 10, *Structure and Properties of MgO and Al_2O_3 Ceramics*. Edited by W. D. Kingery. American Ceramic Society, Columbus, OH, 1984.

[10] P. R. Kenway, “Calculated Structures and Energies of Grain Boundaries in α-Al_2O_3,” *J. Am. Ceram. Soc.*, **77** [2] 349–55 (1994).

[11] W. D. Kingery, “Metal–Ceramic Interactions: IV, Absolute Measurement of Metal Ceramic Interfacial Energy and Interfacial Adsorption of Silicon from Iron–Silicon Alloys,” *J. Am. Ceram. Soc.*, **37** [2] 42–45 (1954).

[12] T. Ikegami, K. Kotani, and K. Eguchi, “Some Roles of MgO and TiO_2 in Densification of a Sinterable Alumina,” *J. Am. Ceram. Soc.*, **70** [12] 885–90 (1987).

[13] C. A. Handwerker, J. M. Dynys, R. M. Cannon, and R. L. Coble, “Dihedral Angles in Magnesia and Alumina: Distributions from Surface Thermal Grooves,” *J. Am. Ceram. Soc.*, **73** [5] 1371–77 (1990).

[14] A. Tsoga and P. Nikolopoulos, “Groove Angles and Surface Mass Transport in Polycrystalline Alumina,” *J. Am. Ceram. Soc.*, **77** [4] 954–60 (1994).

[15] B. L. Adams, S. I. Wright, and K. Kunze, “Orientation Imaging: The Emergence of a New Microscopy,” *Met. Trans. A*, **24** [4] 819–31 (1993).

[16] R. L. Smith, G. S. Rohrer, K. S. Lee, D.-K. Seo, and M.-H. Whangbo, “A Scanning Probe Microscopy Study of the (001) Surfaces of V_2O_5 and V_6O_{13},” *Surf. Sci.*, **367** [1] 87–95 (1996).

[17] D. J. Keller and F. S. Franke, “Envelope Reconstruction of Probe Microscope Images,” *Surf. Sci.*, **294** [3] 409–19 (1993).

[18] J. S. Villarrubia, “Morphological Estimation of Tip Geometry for Scanned Probe Microscopy,” *Surf. Sci.*, **321** [3] 287–300 (1994).

[19] J. S. Villarrubia, “Scanned Probe Microscopy Tip Characterization without Calibrated Tip Characterizers,” *J. Vac. Sci. Technol. B*, **14** [2] 1518–21 (1996).

[20] W. W. Mullins, “Theory of Thermal Grooving,” *J. Appl. Phys.*, **28** [3] 333–39 (1957).

[21] W. M. Robertson, “Grain-Boundary by Surface Diffusion for Finite Surface Slopes,” *J. Appl. Phys.*, **42** [1] 463–67 (1971).

[22] C. A. Handwerker, J. M. Dynys, R. M. Cannon, and R. L. Coble, “Metal Reference Line Technique for Obtaining Dihedral Angles from Surface Thermal Grooves,” *J. Am. Ceram. Soc.*, **73** [5] 1365–70 (1990).

[23] F. C. Frank, “Orientation Mapping,” *Met. Trans. A*, **19** [3] 403–408 (1988).

[24] A. Heinz and P. Neumann, “Representation of Orientation and Disorientation Data for Cubic, Hexagonal, Tetragonal, and Orthorhombic Crystals,” *Acta Crystallogr., Sect. A: Found. Crystallogr.*, **47** [6] 780–89 (1991).

[25] A. Morawiec and D. P. Field, “Rodrigues Parameterization for Orientation and Misorientation Distributions,” *Philos. Mag. A*, **73** [4] 1113–30 (1996).

[26] B. L. Adams, J. Zhao, and H. Grimmer, “Discussion of the Representation of Intercrystalline Misorientations in Cubic Materials,” *Acta Crystallogr., Sect. A: Found. Crystallogr.*, **46** [7] 620–22 (1990).

[27] P. W. Tasker, “Surfaces of Magnesia and Alumina”; pp. 276–89 in Advances in Ceramics, Vol. 10, *Structure and Properties of MgO and Al_2O_3 Ceramics*. Edited by W. D. Kingery. American Ceramic Society, Columbus, OH, 1984.

[28] B. L. Adams, D. Kinderlehrer, W. W. Mullins, A. D. Rollett, and S. Ta’asan, “Extracting the Relative Grain Boundary Free Energy and Mobility Functions from the Geometry of Microstructures,” *Scr. Metall.*, **38** [4] 531–36 (1998). □